geosciences

MDPI

Article

Geomorphometric and Geophysical Constraints on Outlining Drained Shallow Mountain Mires

Stanisław Burliga [1,*], Marek Kasprzak [2], Artur Sobczyk [1] and Wioletta Niemczyk [3]

[1] Institute of Geological Sciences, University of Wrocław, pl. M. Borna 9, 50-204 Wrocław, Poland
[2] Institute of Geography and Regional Development, University of Wrocław, pl. Uniwersytecki 1, 50-137 Wrocław, Poland
[3] Stolowe Mountains National Park, ul. Słoneczna 31, 57-350 Kudowa Zdrój, Poland
* Correspondence: stanislaw.burliga@uwr.edu.pl

Abstract: Long-term draining of peatlands results in transformation of vegetation and obliteration of their morphological features. In many areas, efforts are made to restore the original ecosystems and increase their water retention potential. Using combined analyses of a LiDAR-based digital terrain model (DTM), colour-infrared (CIR) imagery data, ground-penetrating radar (GPR) data and electrical resistivity tomography (ERT) data, we tested the applicability of these methods in outlining the extent and subsurface structure of drained mires located in the Stolowe Mountains National Park area, Poland. The LiDAR-DTMs enabled parameterisation of physiographic features of the mires and determination of their extent, runoff directions and potential waterlogging areas. CIR analysis enabled classification of vegetation types. GPR prospecting revealed the bedrock morphology, thickness and internal structure of the peat deposits, showing that this technique can also provide data on variability in the decomposition of phytogenic deposits. The obtained ERT sections indicate both the thickness of peat deposits and variability in the bedrock internal structure. The results show that integrated analyses of data obtained with different methods can be an effective tool in outlining the original extent of peatlands, with potential application in the planning of peatland ecosystem restitution.

Keywords: drained mountain mires; ground-penetrating radar; electrical resistivity tomography; LiDAR-based digital terrain model; colour-infrared imagery; Stolowe Mountains National Park

Citation: Burliga, S.; Kasprzak, M.; Sobczyk, A.; Niemczyk, W. Geomorphometric and Geophysical Constraints on Outlining Drained Shallow Mountain Mires. *Geosciences* **2023**, *13*, 43. https://doi.org/10.3390/geosciences13020043

Academic Editors: Michela Giustiniani and Jesus Martinez-Frias

Received: 22 November 2022
Revised: 26 January 2023
Accepted: 29 January 2023
Published: 30 January 2023

1. Introduction

The significance of wetlands in local and regional water cycles and their global potential for carbon accumulation have been demonstrated by numerous studies ([1–5] and references therein). Arid seasons occurring worldwide in the last decades have highlighted their role in local water retention by counteracting water deficits within these ecosystems. This potential has been diminished in many areas due to the demand for expanding agricultural use or afforestation of land, as has occurred, for example, in mountain areas in central Europe where many mires were drained in the 19th and 20th centuries. As a consequence of climate change and draining, mires have become more susceptible to wildfires, which are especially difficult to tackle when smouldering fires develop [6,7]. The need for protection of wetlands is undisputable at present, and efforts are being made to restore local hydrological systems and original ecosystems, e.g., by damming drainage ditches, as has occurred in the Stolowe Mountain National Park area in Poland [8,9]. One of the key problems in the protection and restoration of drained mires is that anthropogenic changes have obliterated their morphological and environmental features, making their original boundaries difficult to determine in the field. Moreover, for the majority of mountain mires, their thickness and basement morphology are only roughly known, yet this knowledge is essential for understanding local hydrological systems and, thus, efficient protection of mires.

Using three different mires located over the Stolowe Mountains (central Sudetes) we tested the application of integrating digital elevation models, remote sensing data and

shallow geophysical prospecting methods (electrical resistivity tomography and ground penetrating radar) to delineate the extent of mires, their thickness, internal structure, and basement morphology. Our approach was guided by the effectiveness of those geophysical methods proven in investigations on other wetlands [10–16], the proven applicability of remote sensing in the analysis of diversity of vegetation and monitoring of changes in biodiversity [17,18], as well as the analytical potential of LiDAR-based DTM shown for the Stolowe Mountains National Park in Poland [19].

2. Study Area

The mires under study are located in the Stolowe Mountains (SM), located within the Sudetes of SW Poland, at the NE margin of the Bohemian Massif (Figure 1). This is a stepped tableland where the relief is determined by the architecture of geological layers. The mountains are built of three large-scale bed sets of coarse-grained sandstones (the lower, middle and upper sandstone units) separated by a heterolithic sedimentary succession containing calcareous mudstones and fine-grained sandstones intercalated with claystones [20] of Cenomanian–Coniacian age, deposited in the Cretaceous Basin over the northern flank of the Bohemian Massif [21]. Since the tops of large-scale bedding are gently inclined (up to 5°), the sandstone beds less susceptible to erosion form two distinct plateaus over the area of the SM: (1) the upper plateau situated mostly above 900 m a.s.l., corresponding to the top of the upper sandstone unit and preserved as remnants over small areas of the SM, and (2) the middle plateau rising between 600 m and 790 m a.s.l., morphogenetically linked with the top of the middle sandstone and covered by non-eroded remnants of the fine-grained succession [22]. Such morphology and lithology favoured the development of seasonal and permanent wetlands due to low efficiency of the subsurface drainage. Woronko [23] estimated the total area of wetlands over the SM at ca. 450 ha (152 h of permanent wetlands), which corresponds to ca. 37% of the plateaus. The distribution of the largest permanent wetlands in the SM is shown in (Figure 1). The development of mires was also favoured by climatic conditions. The values of the climatic water balance (CWB) for the meteorological station situated at the foot of the middle plateau (in the village of Słoszów) indicate the predominance of precipitation over potential evaporation [24]. The average annual air temperature on the plateaus of the SM is ca. 4.5 °C, and the average annual rainfall calculated on the basis of a single rainfall station located on the middle plateau (700 m a.s.l.) for the period 1976–2005 was ca. 858 mm [24]. July is the wettest month with an average of 122 mm of rainfall. Although the middle plateau hosts several mires, multiple springs and is drained by a number of small creeks, the river discharge is generally low, increasing primarily during spring thaw. The hydrological system was strongly influenced by human activity for more than 100 years. Since the 19th century, the majority of wetland areas have been drained by a network of ditches for the sake of forest management and agricultural use [23,25,26], which lowered the groundwater table and degraded the mires. This destructive impact on the mire ecosystems ended when the SM National Park was established in 1993 and efforts to restore the original hydrological system began. Activities included damming up the ditches over selected mires to raise the groundwater table [8]. Nevertheless, long-time lowering of the groundwater table degraded the mire ecosystems and enhanced the chemical and physical alteration of organic soils in the artificially increased zone of aerobic conditions [26,27].

The subsurface research over the mires in the SM has focused on two main topics: (1) the palynological record in phytogenic sediments of several mires; and (2) soil analyses over wetland areas. Marek [28], on the basis of six drilled peat profiles, outlined the evolution of vegetation for the area's largest mire, the Wielkie Torfowisko Batorowskie mire, and found that phytogenic sedimentation began at approx. 10,000 BP, and that the phytogenic deposits are locally over 5 m in thickness, being deposited directly on mineral basement in a shallow depression. There are no remnants of flora indicative of a lacustrine environment at any stage of the peat bog evolution. Glina et al. [29] carried out soil and palynological analyses on single profiles drilled in four other areas with peat vegetation,

where the thickness of phytogenic sediments reached a maximum of approx. 80 cm. The obtained data imply that those smaller mires originated in the middle to late Holocene (between 3301 BC to AD 1137 according to radiocarbon dating), and that there was a strong human impact on vegetation since the Middle Ages, enhanced by a drainage network built in the 19th century. Soil studies carried out by [26,27,29–32] revealed internal layering of the phytogenic sediments and their degradation due to draining of the mires. Since all those studies provided information on mire subsurface structure limited to randomly located boreholes, the actual morphology of the phytogenic sediment basement and their internal structure remain unknown.

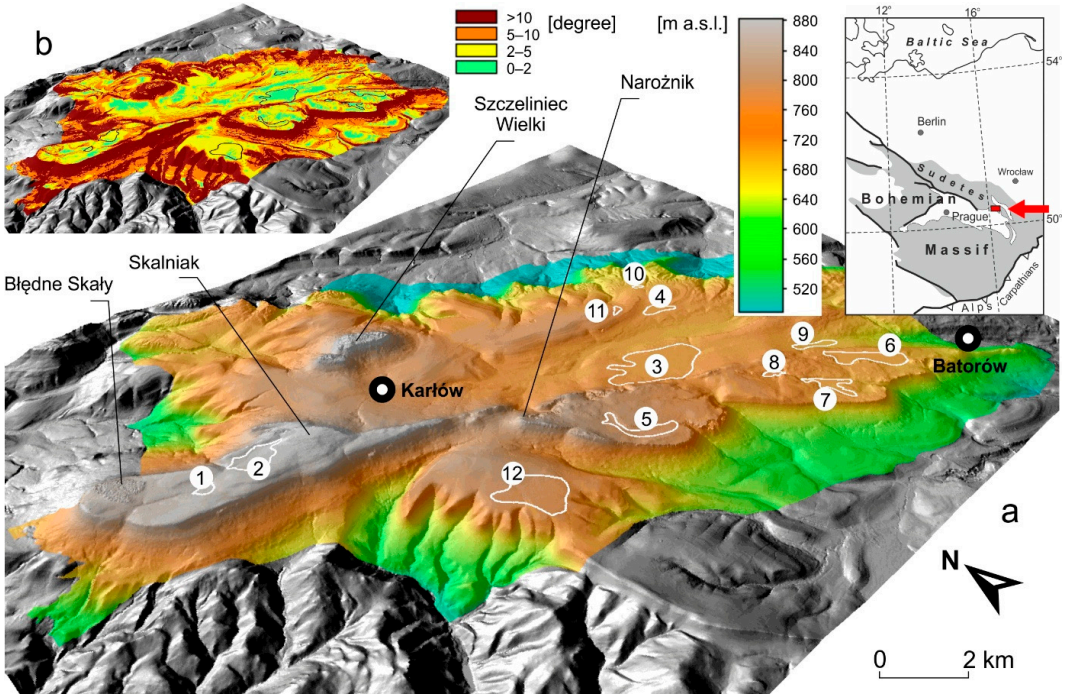

Figure 1. Study area: a—shaded relied DEM of the Stołowe Mountains with wetlands marked: 1—Długie Mokradło (DM), 2—Krągłe Mokradło (Skalniak), 3—Wielkie Batorowskie, 4—Niknąca Łąka (NL), 5—Narożnik–Kamienny Potok, 6—Płaskowyż Batorowa (1), 7—Płaskowyż Batorowa (2), 8—Płaskowyż Batorowa (3), 9—Małe Torfowisko Batorowskie (MTB), 10—Burzowa Łąka, 11—Czeska Łąka, 12—Sawanna Łężycka. Test areas for this study are bolded; b—slope map; c-inset map shows location of the Stołowe Mts. (red rectangle) within the Bohemian Massif, Central Europe.

For this study, three mires were selected, located at various altitudes over two types of bedrock (Figure 1). The Długie Mokradło (DM) mire is situated at an altitude of approx. 849–850 m a.s.l. over the upper morphological plateau, underlain by Coniacian coarse-grained sandstones [20]. The Niknąca Łąka (NL) and the Małe Torfowisko Batorowskie (MTB) mires are situated on the Turonian heterolithic upper succession that comprises the middle morphological horizon of the SM, at altitudes of 714–715 m and 691–694 m a.s.l., respectively. The DM and NL are cut by old drainage ditches which were partly dammed up in 2010–2012, whereas the MTB is still drained by ditches located morphologically below and away from the main mire area. There are no tectonic zones in areas of the three mires [20], making local morphology and hydroclimate the main factors responsible for the origin of the mires.

3. Methods

The three mires were subjected to digital spatial analysis based on morphology and vegetation cover, which was followed by field investigation of their geological structure

using two types of near-surface geophysical techniques: ground penetrating radar (GPR) and two-dimensional electrical resistivity tomography (ERT 2D).

Two types of digital data were used in the study: digital terrain model (DTM) and colour infrared photography (CIR). The DTM was applied to analyse and parametrise the morphology of the mires, while CIR was used to analyse the vegetation on the mire areas.

The DTM was obtained from processing point cloud data from airborne laser scanning (ALS). The classified point cloud with a minimum density of 4 points/m^2 allowed for the construction of the DTM with a resolution of 1 × 1 m, the height accuracy of which is about 0.1 m [33]. The source data were downloaded from the website provided by the Polish Central Office of Geodesy and Cartography (geoportal.gov.pl, public domain). The DTM parameterisation was performed in SAGA GIS software. We relied on four primary and secondary geomorphometric parameters to infer the behaviour of water on the ground surface: hypsometry; total catchment area; topographic wetness index in SAGA modification; and convergence index [34]. Additionally, based on the D8 flow algorithm, a vector layer with flow accumulation was automatically determined. The boundaries of the parameterised areas were positioned at the bases of slopes.

CIR data provided by The Stolowe Mountains National Park were processed in the SAGA GIS software. In order to distinguish various types of vegetation, an unsupervised classification of images distinguished 10 classes. Out of these, we selected 2 classes that most commonly cover wetlands and they are presented in two shades of green on the resulting maps. The proposed procedure is based on experiments in which we tested the number of classes set in unsupervised classification.

Geophysical surveying with the two near-surface methods was carried out twice: on 3 September 2021 after a period of rainfall, and on 28 October 2021, after a few weeks without significant rainfall. The ERT uses the phenomenon of different conductivity of electric current through the subsurface which is conditioned by mineralogical composition, structure and texture of sediments, the presence and mineralization of groundwater and other factors [35–39]. The surveying is conducted by driving electrodes into the ground along a survey line. The electrodes are connected with a multi-core cable and enable multiple measurements to be carried out in the systems of four electrodes: two current (C1, C2) and two potential (P1, P2). The control device allows the electric current to be transmitted through the current electrodes and the voltage to be measured through the potential electrodes. The known intensity of the current, the distance between the electrodes and the coefficient k, depending on the adopted measurement method, enable the determination of the value of soil resistivity at a given point in the profile. Combinations of such electrode arrays allow standard sounding and geoelectric profiling. Since the potential measured on the surface of the layered rock body is an average value, based on the acquisition (measurements), it is possible to provide only the apparent resistivity values for certain depths. In order to obtain the distribution of real (interpreted) resistivity, inversion modelling is performed [40].

We used an ARES II device and a set of 80 electrodes over a distance of 79 m. The one meter spacing between the electrodes facilitated the visualization of thinner layers of peat. The course of the measurement sections was designed in such a way as to examine the places with the thickest accumulations of peat as well as the wetland margins. Nevertheless, each of them was conditioned by the ability to move in the field. In the case of the MTB, the acquisition line cross-cut a relief form resembling a peat dome. Two fieldwork dates allowed the measurement to be repeated exactly along the same measurement line in order to investigate the potential effects of moisture differences in the substrate. Measurements were collected using the Schlumberger method, which is considered to be relatively universal in recognizing both vertical and horizontal structures in the subsurface [41]. The obtained results were subjected to smooth inversion (L2) in the RES2DINV software (Geotomo, Malaysia), taking into account the topographic correction. The modelling results were presented in log resistivity for the 5th iteration in the Surfer software (Golden Software),

which gives greater possibilities of interpolation and manipulation of colours than in the Red2Dinv.

Ground-Penetrating Radar (GPR) is a high-resolution geophysical method based on the emission of ultra-short wavelength electromagnetic energy into the soil medium, which is attenuated, reflected and refracted on the surfaces of layers with different dielectric properties, and the travel time to a reflecting horizon is simultaneously registered by the receiving antenna [42,43]. We carried out the GPR surveys with the use of a shielded Ramac II (Mala) radar with an antenna frequency of 250 MHz, applying a rotating wheel for mechanical measurement of the profile length and locating the beginning and the end of the GPR profile with a precise GPS receiver (differential GPS) with a horizontal resolution of ~1–2 m. For each mire, the profiles were led in a grid of lines parallel and perpendicular to each other and also parallel to the ERT profiles (Figure 2). In this paper, we present a detailed analysis of two representative profiles for each mire.

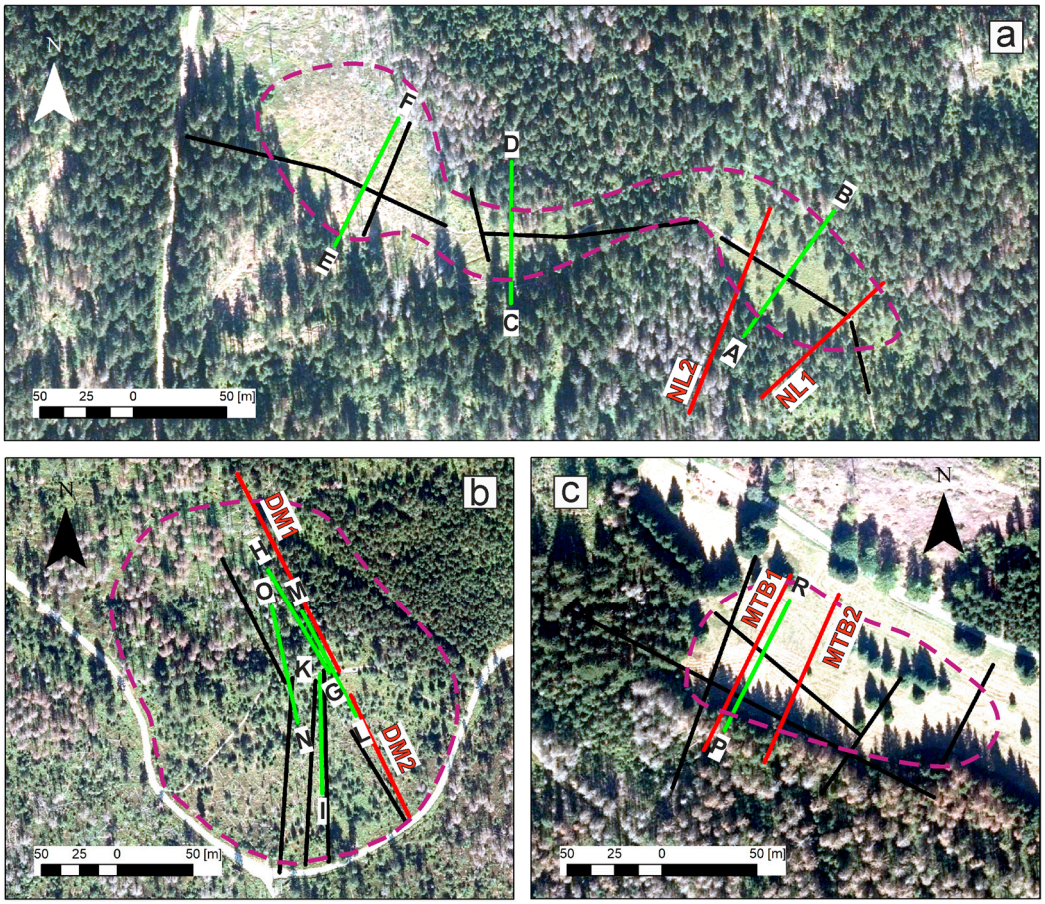

Figure 2. Location of ERT (green lines) and GPR (red lines) profiles analysed for (**a**) NL mire, (**b**) DM mire and (**c**) MTB mire in the SM. The black lines are GPR profiles (not presented in this paper). The dashed purple lines are the approximate mire boundaries based on literature and analyses of GIS materials.

To determine the depth of the individual horizons on the echograms using the TWT (two-way travel time) method, the value of $\varepsilon = 64$ (F/m) was adopted for the dielectric constant, which determines the conductivity typical for saturated peat and is a direct derivative of the EM wave attenuation [42]. The speed of propagation of the electromagnetic wave in the medium was established based on the relationship:

$$v = c / \sqrt{\varepsilon} \quad (1)$$

where v is the speed of propagation of an electromagnetic wave in the medium, c is the speed of light in a vacuum, and ε is the dielectric constant.

The calculated speed of electromagnetic wave propagation with the value of electric permeability ε = 64 was 0.0375 m ns^{-1}, and this value was then used to compare with the peat core information to determine the depth on the echograms. The GPR data were processed in REFLEXW v.8.5 (Sandmeier, Germany) and Prism 2 (Radar Systems Inc., Riga, Latvia). The GPR data filtration was preceded by a procedure for correcting the time-zero point of the first reflection surface for an electromagnetic wave, made via single route analysis, to eliminate direct waves forming due to antenna–air layer–mire surface interference. The data processing (filtering) carried out in the next stage was aimed at: (1) eliminating background noise (filters: background removal, horizontal LP-filter), (2) image averaging (median filter), and (3) signal amplification (gain function) in order to obtain images useful for further geological interpretation.

4. Results and Interpretation

4.1. Physiography of Mires

4.1.1. DTM/LiDAR Data Analysis

The analysis of the terrain surface of the three mires based on LiDAR data allows for the identification of their individual topographic and hydrographic features (Table 1). The NL bog is situated over an extensive flat area and is the least transformed by drainage ditches; hence, the potential surface runoff can be partially realized by a network of shallow channels in a dendritic system (Figure 3a,b). Water concentration is favoured in the central part of the mire, and there are two possible outlets: towards the S and SE (Figure 3c,d). The DM bog is the most impacted by drainage ditches, which have completely modified the potential surface runoff (Figure 3a,b). There are distinct elongated concave forms on the mire surface, which under natural conditions would favour water concentration, implying two possible outlets, i.e., towards the west (Figure 3c,d). The MTB mire is situated in a relatively narrow valley where surface runoff is conditioned by drainage ditches (Figure 3a,b). Under natural conditions, the concentration of water would be mainly favoured in the zone close to the valley axis, with the outlet towards the SE (Figure 3c,d). Figure 3d indicates that there is a peculiar convex morphological feature situated above the valley axis and below a line of springs located over the north-western slopes in the head of the valley. Field studies showed that this morphological form correlates with the occurrence of typical mire vegetation.

4.1.2. Colour-Infrared Imagery Processing

The effect obtained by automatic classification of near-infrared images is strongly dependent on the area covered with tree vegetation (Figure 4). Although the images show that the mires are dominated by trees, there are also non-forested areas. Over the NL mire, there are four elongated, non-forested fields, with the largest of them extending into the central part of the mire. It is distinguished in unsupervised classification as a separate class, and displayed by us in dark green colour in Figure 4a. Similarly, a treeless compact area is noticeable on images in the central part of the DM mire and is marked in dark green in Figure 4b. The classification result obtained for the MTB mire is more unequivocal due to the deforestation of this area. The majority of the vegetation belongs to one class represented by a dark green colour. Only in the western part of the mire is there an area belonging to the class marked with light green (Figure 4c), which is the bulge zone indicated by the LiDAR DTM (Figure 3d) and that we correlated with mire vegetation during the field inspection.

4.2. Subsurface Structure of Mires

4.2.1. Ground-Penetrating Radar Data Analysis

The GPR measurements with the RAMAC II device were carried out along longitudinal and transverse profiles with respect to the elongation of the mires and the dominant surface

water runoff trend (Figure 3). The location of the profile lines is shown in Figure 2. In the NL mire, we acquired one longitudinal and five transverse profiles and in the MTB mire, one longitudinal and three oblique profiles. In the DM mire, we measured seven profiles trending obliquely to the axis of the morphological depression, due to the presence of numerous ditches, fallen trees and shrub vegetation, which prohibited continuous profiling in a direction concordant with the water runoff. We present the two most representative examples of the geometry and internal structure for each mire in Figure 5.

The subsurface image of the NL mire on the radargrams revealed the presence of a shallow depression filled with peat deposits (Figure 5a–d). The width of this symmetrical depression along the NL1 profile is approx. 100 m and is ca. 80 m along the NL2 profile. The base surface is uneven, indicative of an erosional origin of the depression. The topmost part of the mire basement consists of whitish, weakly permeable clay–silt material. The maximum depth to the mire bottom implied by the radargrams is ca. 125 cm (NL1 profile), which is close to the thickness measured with a hand probe (ca. 115 cm). The horizontal and relatively continuous reflections noticeable within the depression infill point to horizontal stratification of the peat deposits, as revealed by the performed coring tests and reported NL mire internal structure [29].

Table 1. Results of the mire surface topographic analysis based on LiDAR DTM.

Geomorphometrical Parameter	Site		
	NL Mire	DM Mire	MTB Mire
Hypsometry and automatic determination of surface runoff (streams)	• Almost flat surface; • Minimal slope of the surface towards S and SE.	• The mire occupies a valley depression; • Difference in height is over 5 m; • Surface runoff towards W.	• The mire occupies a valley depression; • The difference in height is over 15 m; • Surface runoff towards SE.
Total catchment area	• Surface runoff mainly through natural depressions; • Surface runoff in the dendritic network.	• Surface runoff is realized through a network of drainage ditches; • A parallel outflow network dominates.	• Main runoff lines correlate with the drainage ditches; • The inflow to the drainage ditches in the dendritic network.
Topographic wetness index	• Areas topographically predisposed to water concentration are located in the central part of the mire.	• Areas topographically predisposed to water concentration form elongated zones in the central and southern part of the mire.	• Areas topographically predisposed to water concentration form an elongated zone near the valley axis.
Convergence index	• There are no extensive concave and convex forms on the mire surface; • The mire is delineated to W, N and E by slop bends.	• The largest concave form is situated in the eastern part of the mire; • The mire is clearly delineated in morphology by valley slopes.	• There is an isolated convex form in the topography of the western part of the mire; • The mire is clearly delimited by the valley slopes.

The radargrams acquired for the DM mire indicate that its southern border is delimited by a relatively sudden lowering of the bedrock, as shown on the DM2 profile at a distance of ca. 25 m from the beginning of the profile (Figure 5e,f). The northern border is less clear, being located at a distance of ca. 45 m from the beginning of the radargram DM1, where undulations in the mire base disappear. Thus, the radargrams document the presence of wide (90–100 m), asymmetric, trough-shaped depression filled with horizontally stratified peat deposits with a maximum thickness of ca. 100 cm, and this thickness was also

confirmed by hand probing (98 cm). The base surface of the mire is relatively even. Clay-to-sand sediments of whitish colour were documented by probing below the peat deposits.

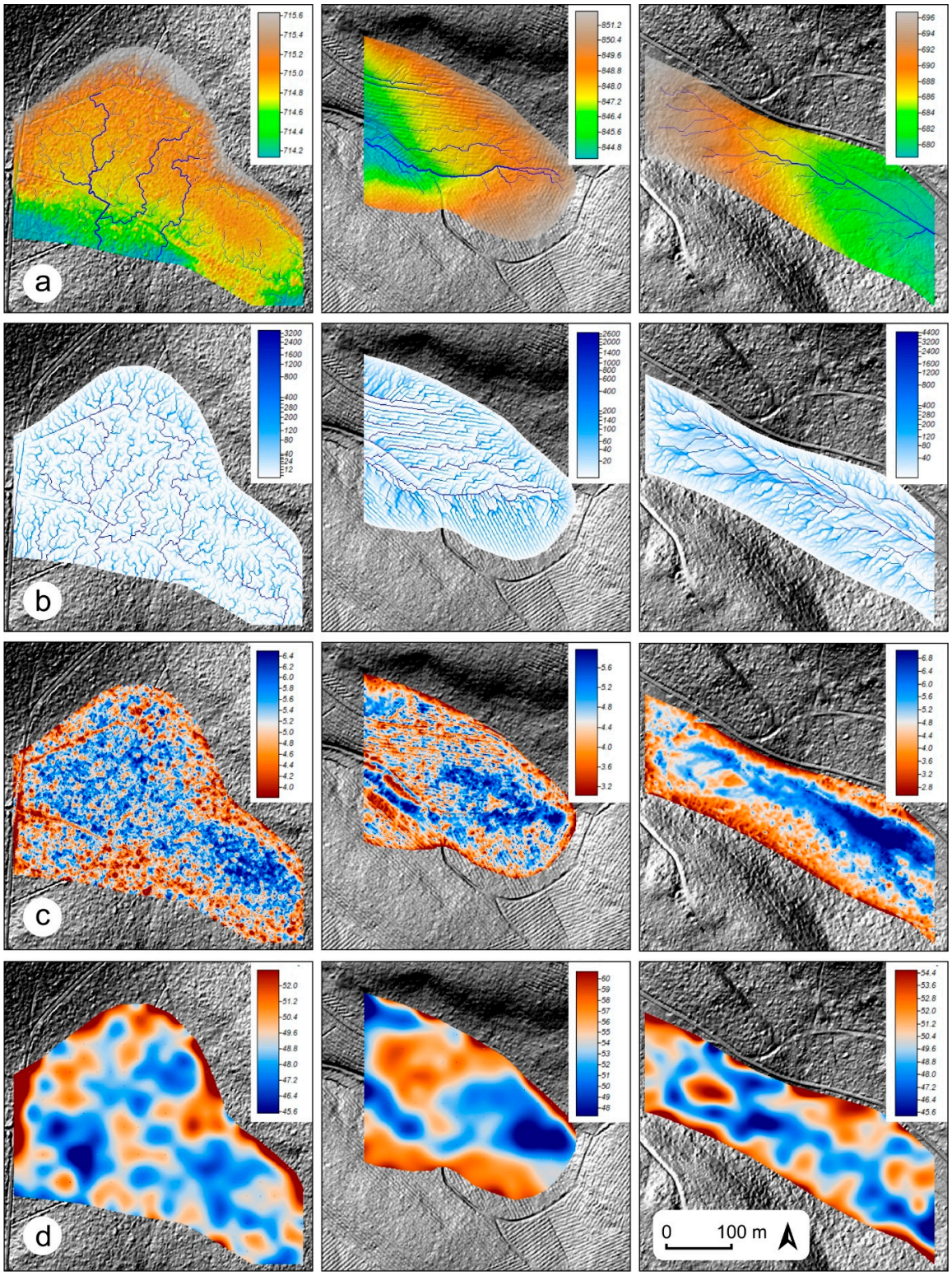

Figure 3. Geomorphometric parameterisation based on LiDAR DTM for the NL, DM and MTB mires (in columns from left to right, respectively): (**a**)—hypsometry (in metres a.s.l.) and automatic determination of surface runoff (streams in blue), (**b**)—total catchment area (in square metres), (**c**)—topographic wetness index in SAGA GIS modification, and (**d**)—convergence index.

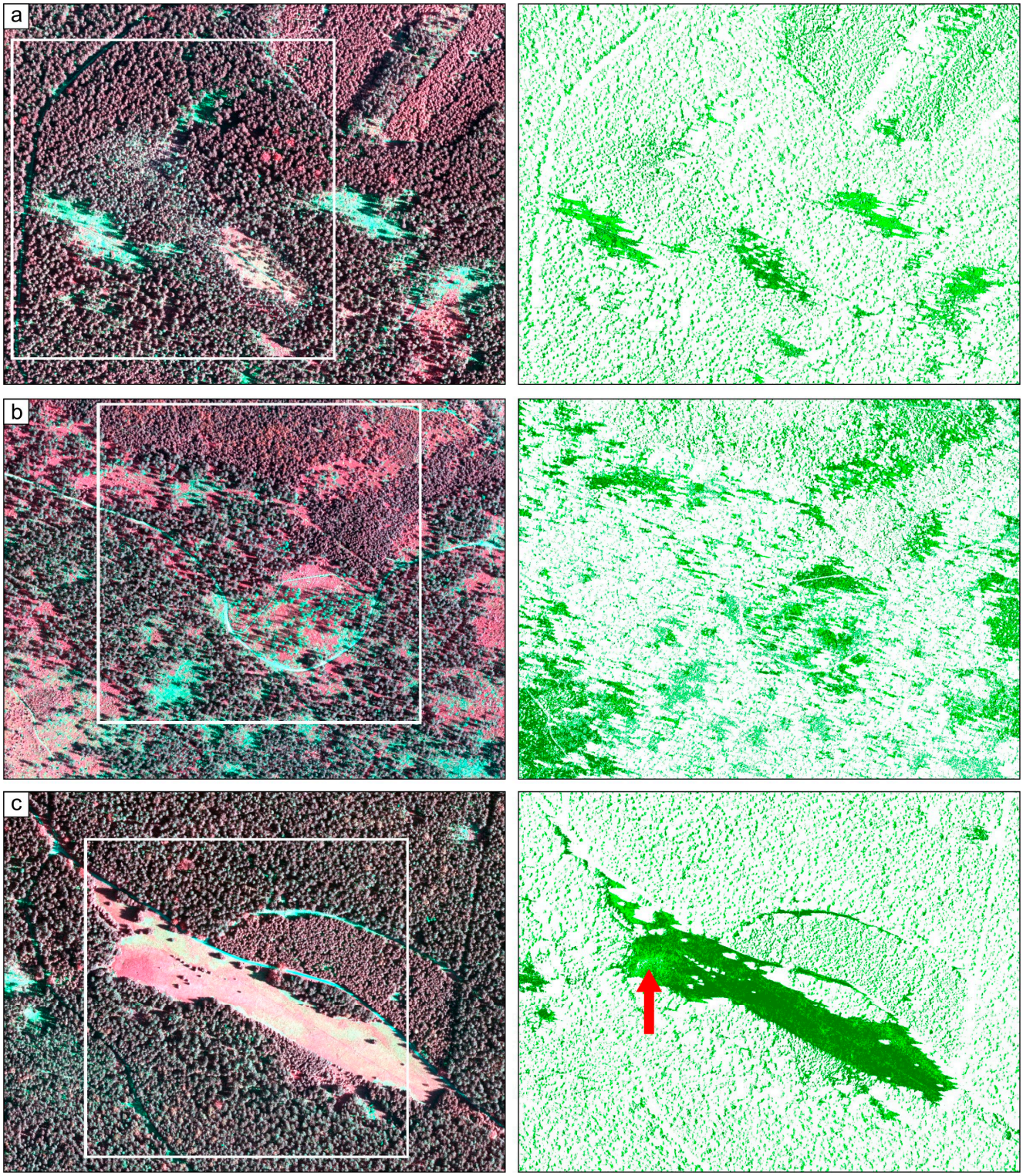

Figure 4. Colour-infrared (CIR) imagery of mire areas in the SM (**left** column) and the two classes out of a set of 10 of automatic vegetation classifications, displayed as light and dark green (**right** column, explanations in the text): (**a**)—NL mire, (**b**)—DM mire, (**c**)—MTB mire. White boxes on the images in the left column indicate the areas shown in Figure 3. The red arrow indicates the bulged surface in the MTB with typical mire vegetation.

The MTB mire developed in a morphological depression is bordered from the south and north by a step-like rise in the bedrock, with the boundaries trending approximately

WNW–ESE, i.e., subparallel to the axis of the valley (Figures 3 and 5i,j,k,l). The width of the depression is ca. 70 m in the western part of the mire and diminishes to ca. 50 m to the east. The base surface of the mire is uneven, showing gentle undulations and a central rise dividing the mire into two subbasins. The maximum thickness of phytogenic deposits indicated by radargrams is ca. 100 cm (95 cm according to hand probing). There are horizontal and wavy-to-lenticular reflections in the phytogenic infill of the depression, indicative of varying types of layering within these deposits. Below the mire infill, whitish clay–mud–sand sediments with sandstone pebbles were documented, and the field inspection showed that a few sandstone boulders occur on the mire surface.

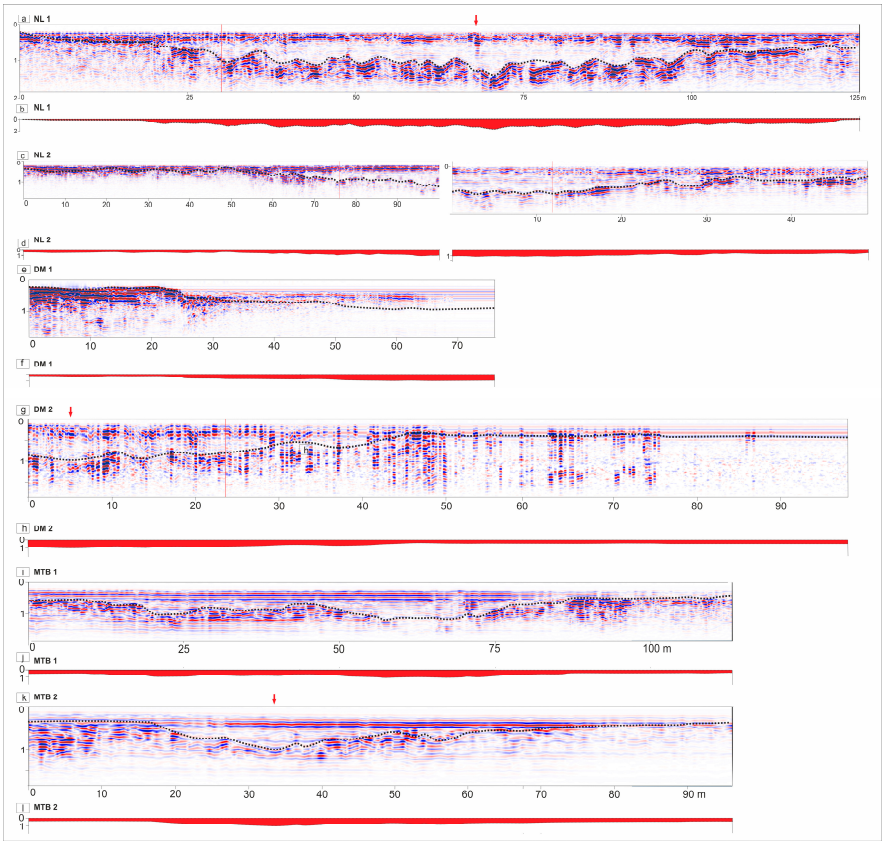

Figure 5. Subsurface structure of the NL, DM and MTB mires from radargrams obtained with a RAMAC II and processed with REFLEXW software: (**a**,**c**) show the profiles NL1 and NL2 with the geometry of phytogenic deposits shown in (**b**,**d**); (**e**,**g**) show the profiles DM1 and DM2 with respective geometry of phytogenic deposits in (**f**,**h**); (**i**,**k**) show the profiles MTB1 and MTB2 with the geometry of phytogenic deposits shown in (**j**,**l**), respectively. Locations of profiles are shown in Figure 2. The vertical scale exaggerated in (**a**,**c**,**e**,**g**,**i**,**k**), whereas in (**b**,**d**,**f**,**h**,**j**,**l**), the vertical and horizontal scales are uniform. Dotted lines indicate the base surface of the mire basins, delineated in the echograms in correlation with the hand probing data. The base of the phytogenic deposits coincides with the first stronger reflection under the low-reflection peat layer. Red arrows indicate sites where peat thickness was checked with a hand probe.

4.2.2. ERT Data Analysis

The data from ERT measurements were used to construct eight inversion models showing the shallow geological structure of the three mires. In order to directly compare the obtained results with different resistivity values, inversion models are presented using Log Resistivity (Figure 6).

The horizons interpreted as phytogenic sediments are reproduced on all inversion models near the ground surface. In the models for the NL and DM mires, the mire deposits have clearly lower resistivity (ranging between 20 Ω·m and 300 Ω·m) than the mineral

deposits and solid rocks imaged in the deeper parts of the subsurface. In most cases, the base of these sediments can be clearly determined, as they contrast with the higher resistivity measured for the underlying fine-grained complex rocks or sandstones. There is a distinct difference in the distribution of resistivity in the models for the MTB mire, where low resistivity was measured ($\rho < 200\ \Omega\cdot m$) across the whole profile. In addition, the model obtained for this section had a large RMS error, indicating the difference in measured and calculated resistivity values.

The inversion models indicate a small thickness of phytogenic sediments. This is well illustrated by the case of the DM mire, where it reaches approx. 1–1.5 m (Figure 6). The models show that the spatial extent of peat occurrence can be determined based on the ERT measurements. The limits of the near-surface zone of low resistivity correlate with the mire boundaries displayed by GPR profiles (Figures 5 and 6).

The interpretation of some of the inversion models is not always unambiguous. In the western part of the NL mire (Figure 6, sections CD and EF), the subsurface layer of low resistivity reaches 3–4 m below the ground level. Since the previous work [29] and our field and GPR studies identified the thickness of the phytogenic sediments as < 2 m, we cannot interpret the whole low-resistivity zone as a peat material. In addition, in the EF section, very low resistivity was also visualized much deeper below the ground surface. Because low resistivity can also result from a saturation of sediments with water, we attribute these anomalous low-resistivity horizons to well-watered mineral formations. Such an interpretation is supported by the inversion model for the MTB mire, section PM, where shallow phytogenic sediments do not contrast in resistivity with the underlying mineral sediments.

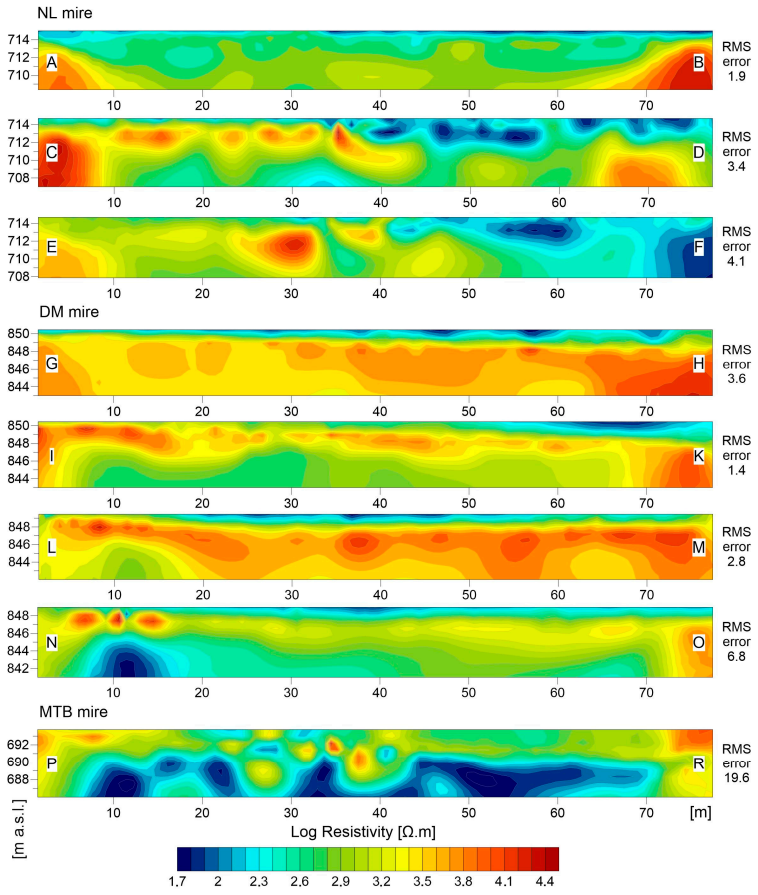

Figure 6. ERT inversion models for the NL, DM and MTB mires. Profile location in (Figure 2).

5. Discussion

5.1. Surface vs. Subsurface Boundaries of the Mires and Their Physiography

Many decades of draining of the studied mires has resulted in changes in vegetation over their surface and the dominance of forest over wetland flora. Even 10 years after damming the drainage ditches, the return of typical mire vegetation seems to be slow, as indicated by the limited areas with non-forest vegetation shown on the CIR images (Figure 3). Although we cannot directly infer how the changes in the vegetation progressed over last 10 years due to the lack of comparative data, the results of our CIR analyses can be useful in such an analysis in future.

The morphometric analysis showed that each mire has a different morphology. The DM mire has a dense network of ditches, well visualised in the digital terrain model obtained from the LiDAR data (Figure 3). The ditch network indicates that the ditches still play a role in the drainage of the uppermost part of the mire and is likely the main cause of the slow readvancement of peatland vegetation over the mire area, as well as of the lack of a fibric peat layer on the surface of the mire [29]. Consequently, the near-surface hemic peat layer continuously favours the growth of tree and shrub vegetation. The presence of the hemic layers near the surface and close to it in the DM and NL mires implies that the mire morphology has been transformed because of peat decomposition and the resulting surface subsidence, which is quite expected when the bulk volume of phytogenic deposits diminishes. The almost flat morphology of the NL mire (Figure 3) provides a hint that the degradation processes triggered by the drainage have ceased and that uniform waterlogging contributes to a wider extent of modern peatland vegetation than in the DM mire. This interpretation is supported by the results of parameterization of the mire surfaces and the TWI and convergence index parameter maps (Figure 3), showing where the best conditions for water concentration on the surface are currently found.

To date, apart from the MTB mire, there are no domed structures in the morphology of the mires typical of peatland ecosystems, and the majority of the mire areas are covered with trees and shrub vegetation. Nevertheless, the integration of LiDAR data analyses with GPR and ERT surveying also proved to be and effective method to delineate both the ancient and potential mire extents. The LiDAR DTM data analyses provided objective information on the physiography of the mires (Figure 3), even though they seem relatively flat in the field and the peat surface is obscured by growing plants. The models of likely hydrographic networks and presumable water runoff directions can be utilized in projects designed to increase water retention in the mire areas. Topographic wetness and convergence indexes hint at the probable mire extent on the surface before their draining and to boundaries that will develop once ditch drainage ceases completely. We assume that the lowermost areas of the mires favour the fastest readvance of wetland vegetation since such a relationship is suggested by the current extent of peat vegetation over the NL mire. The subsurface boundaries of the mires visualised by shallow geophysical prospecting are relatively well defined in all cases, showing that the original depressions hosting the mires have smaller extents than those indicated by LiDAR DTM analysis. This observation provides evidence on the progressive expansion of mire ecosystems and overlapping of phytogenic deposits over a much larger area than the initial peat basins, and thus, also points to increasing water retention potential in these areas over time.

5.2. Geological and Palaeomorphological Constraints for Mire Development

The mires originated over flat or gently inclined surfaces resulting from the tabular arrangement of Cretaceous beds. In all three mires, whitish, fine-grained clastic sediments dominated by clay, silt and fine sand fractions were documented underneath the phytogenic succession. The whitish and pale grey colours are typical for weathered fine- and coarse-grained Cretaceous clastic rocks over the SM, which implies that before the mire ecosystem development, bare mountains left after the last glacial period were eroded and the saprolite was deposited in the morphological depressions. Because of difficulties with hand probing of the bedrock (single probing in the thickest peat area in each mire was carried out), we

infer that the layer of soft mineral deposits is <0.5 m. On the other hand, the ERT profiles display low resistivity rocks of up to 4 m in thickness in the NL mire and 2 m in the DM mire (Figure 6), which may indicate a much thicker accumulation of redeposited saprolite in some areas of those mires. The overall subhorizontal arrangement of high and low resistivity layers on ERT profiles correlates well with the inclination of the Cretaceous beds. Therefore, we interpret the occurrence of a low resistivity layer deeper below the MTB mire as a change in the lithology of the Cretaceous beds. Irrespective of the deeper basement structure and lithology, it is clear that the mires originated over weakly permeable deposits, built predominantly of clays and muds accumulated in erosional depressions. The shapes of these depressions were, at least partly, controlled by tectonic features of the Cretaceous rocks, as can be inferred from the linear trend of the step-like rise of the bedrock near the mire boundaries of the DM and MTB mires (Figure 5). In the absence of documented fault zones near the mires [20], their linear boundaries most probably result from the jointing of interlayering fine- and coarse-grained Cretaceous beds and enhanced initial erosion of these beds in the axial parts of valleys hosting the mires. This interpretation is supported by the occurrence of sandstone pebbles and boulders over the MTB mire, with blocks of sandstone layers are scattered on the mire surface. The base surfaces of the mires are gently concave and uneven (Figure 5), which may result both from the variable erosional incision into the bedrock or, alternatively, from the morphology of depositional structures developed in the valleys prior to the phytogenic deposition. Some roughness of the base surface noticeable on radargrams may also reflect the occurrence of sandstone boulders, similar to those evidenced on the modern MTB surface.

5.3. Internal Structure of Mires

GPR provided information both on the overall geometry of the phytogenic sediments and their internal structure. All three mires are half-lenticular in cross-section, with the base surfaces relatively symmetric in the NL and DM mires and asymmetric in the MTB mire (Figure 5). They are all shallow peat basins, with only a ca. 1 m thick succession of phytogenic sediments accumulated until now. The radargrams show that in spite of the low thickness, different types of reflectors appear in the phytogenic succession. In the NL and DM mires, horizontal reflectors are separated by layers with more discontinuous reflection patterns, while in the MTB mire, there are also wavy and lenticular patterns of reflections. Based on the comparison of the results of soil studies carried out on the NL and DM mires by Glina et al. [29] and our radargrams, we conclude that the different patterns of reflectors correspond to variability in the decomposition of organic matter in the phytogenic succession. The correlation between the peat types and GPR profile for the NL mires is illustrated in Figure 7. Glina et al. [29] identified variably decomposed layers of peat in a single core from the NL mire and distinguished (in the order of a degree of peat decomposition) fibric, hemic and sapric peat layers. Although our GPR profiles do not cross-cut the soil logging site, the succession of peat layers matches various patterns of reflectors. Fibric peat layers correlate with chaotic reflections, whereas hemic and sapric ones are imaged as more continuous horizons (Figure 7). This observation also applies when comparing the soil profile of Glina et al. [29] for the DM mire and our radargrams. Hence, radargrams seem to be useful in rough identification of variability in peat decomposition in phytogenic successions. This was already suggested for other peatlands [11,44–46]; however, as the peat thickness was there much greater, the resolution was lower. Our tests show that in shallow mires, the obtained resolution of the internal structure of the phytogenic deposits can be quite high. Based on the relationship shown in Figure 7, we infer a rather thin layer of fibric peat in the MTB mire and the dominance of more decomposed peat in the phytogenic succession. However, the presence of wavy and lenticular reflectors in the MTB mire, as well as the occurrence of sandstone boulders, may imply that phytogenic deposits interlayer with debris flow deposits and slope tills which are redeposited from the slopes to the valley bed. To verify this concept, further studies with the use of invasive methods would be required. Nonetheless, the horizontal

depositional patterns indicate that the three analysed mires developed under relatively stable water conditions, possibly in an environment of stagnant waterlogging, enabling uniform growth of phytogenic layers over the entire mire area.

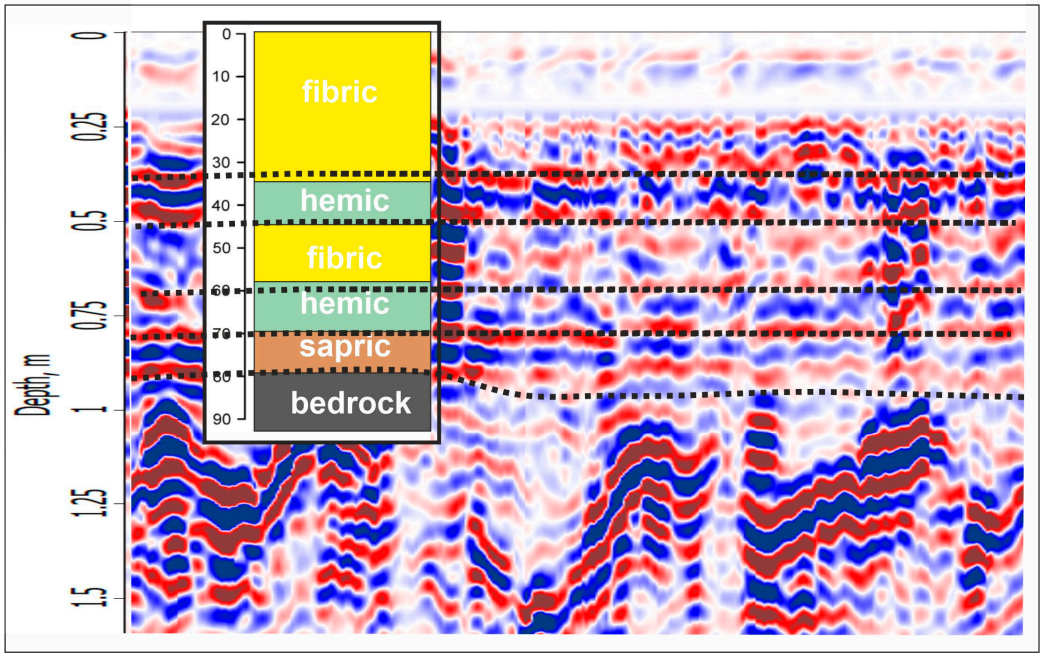

Figure 7. Schematic correlation of reflector patterns on radargrams with the soil profile (overlaid column), as interpreted by Glina et al. [29] for the NL mire. Fibric, hemic and sapric are types of peat.

6. Conclusions

Sustained drainage of mountain mires over the Stolowe Mountains National Park area in the last century resulted in significant transformation of their morphology, vegetation and in partial decomposition of peat deposits. As a result, it is difficult to outline the former boundaries of the mires in the field without the application of invasive methods, the use of which is highly restricted in conservation areas. Our study demonstrates that this obstacle can be overcome by the integration of various methods of non-invasive prospecting, including LiDAR and remote sensing data analyses and near-surface geophysical methods.

The LiDAR-based DTM of the mire surface is particularly useful in delimitating the most probable mire boundaries inferred from physiographic features as well as the identification of directions of surface runoff and areas most prone to waterlogging. Such knowledge is invaluable when projects of mire ecosystem restoration are considered or an increase in water retention over a peatland area is targeted. Although the analyses of CIR data did not help in outlining the current extent of the studied mires due to the presence of tree and shrub vegetation, this method seems to be extremely valuable in comparative studies of changes in vegetation over longer periods if CIR or comparable data from different years are available.

Near-surface geophysical methods are essential for a non-invasive identification of mire thickness and subsurface architecture. All three mires appeared to be shallow and developed in depressions formed in the bedrock due to erosion of the Upper Cretaceous sedimentary rocks. Their development was primarily conditioned by a weakly inclined arrangement of the bedrock layers consisting of fine-grained, weakly permeable clastic rocks and their location near spring zones. The depth values obtained by manual probing indicate the accuracy of depth determinations with the GPR method to be within 5 to 10%. Apart from the well-known potential of high-resolution imaging of the peat–mineral basement contact with GPR, the technique also proves to be useful in identifying variously decomposed peat layers in the phytogenic succession. The wider extent of the

uppermost horizontal reflectors on radargrams than the morphological depression in the bedrock provides evidence of progressive expansion of the peatland ecosystem in the mires, which were destroyed by draining in the last century. On the other hand, it implies the possibility of increasing the water retention potential of the mires and area covered by wetland vegetation, at least to their pre-draining extent, if artificial drainage of the mires is eliminated. The thickness of the phytogenic succession in the mires is low, below 1.5 m according to both the GPR and ERT prospecting results. Better approximation to hand probing results is obtained from the GPR prospecting; however, the ERT profiles also provide data on the deeper basement, such that the overall types of rocks and their arrangement can be deduced if local stratigraphy and tectonics are known. It is necessary to note that ERT investigations of shallow mires requires acquisition with tight spacing between the electrodes (every 1 m). Nonetheless, the knowledge of peat thickness distribution over the mires and their basement morphology is worth any effort since, on the basis of this information, appropriate management plans for peatland restoration can be formulated as well as more effective protection procedures implemented in the case of human-induced threats to these ecosystems.

Author Contributions: Conceptualization: S.B., W.N.; methodology: M.K., A.S., S.B.; field investigation: S.B., M.K., A.S., W.N.; GPR investigation: A.S. and S.B.; ERT investigation, CIR and LiDAR-based DTMs analyses: M.K.; result analysis: S.B., M.K., A.S., W.N; writing—original draft preparation: S.B., M.K. and A.S.; writing—review and editing: S.B., M.K. and A.S.; project administration: S.B., W.N. All authors have read and agreed to the published version of the manuscript.

Funding: This research was supported in 2021 by the Polish Forest Fund, General Directorate of State Forests, Warsaw, Poland.

Data Availability Statement: Digital data were made available by the Central Office of Geodesy and Cartography in Poland (available on geoportal.gov.pl, public domain). The CIR images were made available for study by the Stolowe Mountains National Park.

Acknowledgments: The authors would like to thank G.D. Hoke for valuable comments to the early version of the paper. The authors thank the anonymous reviewers, whose remarks helped in the final text improvement.

Conflicts of Interest: The authors declare no conflict of interest.

Abbreviations

GPR	ground penetrating radar
ERT	electrical resistivity tomography
CIR	colour-infrared imagery
SM	Stołowe Mountains
NL	Niknąca Łąka mire
DM	Długie Mokradło mire
MTB	Małe Torfowisko Batorowskie mire

References

1. Botch, M.S.; Kobak, K.I.; Vinson, T.S.; Kolchugina, T.P. Carbon pools and accumulation in peatlands of the former Soviet Union. *Glob. Biogeochem. Cycles* **1995**, *9*, 37–46. [CrossRef]
2. Page, S.E.; Siegert, F.; Rieley, J.O.; Boehm, H.-D.V.; Jaya, A.; Limin, S. The amount of carbon released from peat and forest fires in Indonesia during. *Nature* **2002**, *420*, 61–65. [CrossRef] [PubMed]
3. Holden, J. Peatland hydrology and carbon release: why small-scale process matters. *Philos. Trans. R. Soc. A: Math. Phys. Eng. Sci.* **2005**, *363*, 2891–2913. [CrossRef] [PubMed]
4. Limpens, J.; Berendse, F.; Blodau, C.; Canadell, J.G.; Freeman, C.; Holden, J.; Roulet, N.; Rydin, H.; Schaepman-Strub, G. Peatlands and the carbon cycle: from local processes to global implications—A synthesis. *Biogeosciences* **2008**, *5*, 1379–1419. [CrossRef]
5. Loisel, J.; Gallego-Sala, A.V.; Amesbury, M.J.; Magnan, G.; Anshari, G.; Beilman, D.W.; Benavides, J.C.; Blewett, J.; Camill, P.; Charman, D.J.; et al. Expert assessment of future vulnerability of the global peatland carbon sink. *Nat. Clim. Chang.* **2020**, *11*, 70–77. [CrossRef]

6. Watts, A.C.; Kobziar, L.N. Smoldering Combustion and Ground Fires: Ecological Effects and Multi-Scale Significance. *Fire Ecol.* **2013**, *9*, 124–132. [CrossRef]
7. Sulwiński, M.; Mętrak, M.; Wilk, M.; Suska-Malawska, M. Smouldering fire in a nutrient-limited wetland ecosystem: Long-lasting changes in water and soil chemistry facilitate shrub expansion into a drained burned fen. *Sci. Total. Environ.* **2020**, *746*, 141142. [CrossRef]
8. Jermaczek, A.; Wołejko, Ł.; Chapiński, P. *Mokradła Sudetów Środkowych i ich Ochrona (Wetlands of the Central Sudetes and Their Conservation)*; Wyd. Klubu Przyrodników: Świebodzin, Poland, 2012.
9. Glina, B.; Bogacz, A.; Mendyk, Ł.; Bojko, O.; Nowak, M. Effectiveness of restoration of a degraded shallow mountain fen after five years. *Mires and Peat* **2018**, *21*, 1–15. [CrossRef]
10. Slater, L.D.; Reeve, A. Investigating peatland stratigraphy and hydrogeology using integrated electrical geophysics. *Geophysics* **2002**, *67*, 365–378. [CrossRef]
11. Sass, O.; Friedmann, A.; Haselwanter, G.; Wetzel, K.-F. Investigating thickness and internal structure of alpine mires using conventional and geophysical techniques. *Catena* **2010**, *80*, 195–203. [CrossRef]
12. Comas, X.; Terry, N.; Slater, L.; Warren, M.; Kolka, R.; Kristiyono, A.; Sudiana, N.; Nurjaman, D.; Darusman, T. Imaging tropical peat lands in Indonesia using ground-penetrating radar (GPR) and electrical resistivity imaging (ERI): implications for carbon stock estimates and peat soil characterization. *Biogeosciences* **2015**, *12*, 2995–3007. [CrossRef]
13. Walter, J.; Hamann, G.; Lück, E.; Klingenfuss, C.; Zeitz, J. Stratigraphy and soil properties of fens: Geophysical case studies from northeastern Germany. *Catena* **2016**, *142*, 112–125. [CrossRef]
14. Kowalczyk, S.; Żukowska, K.A.; Mendecki, M.J.; Łukasiak, D. Application of electrical resistivity imaging (ERI) for the assessment of peat properties: a case study of the Całowanie Fen, Central Poland. *Acta Geophys.* **2017**, *65*, 223–235. [CrossRef]
15. Walter, J.; Lück, E.; Heller, C.; Bauriegel, A.; Zeitz, J. Relationship between electrical conductivity and water content of peat and gyttja: implications for electrical surveys of drained peatlands. *Near Surf. Geophys.* **2019**, *17*, 169–179. [CrossRef]
16. Pezdir, V.; Čeru, T.; Horn, B.; Gosar, M. Investigating peatland stratigraphy and development of the Šijec bog (Slovenia) using near-surface geophysical methods. *Catena* **2021**, *206*, 105484. [CrossRef]
17. Ihse, M. Colour infrared aerial photography as a tool for vegetation mapping and change detection in environmental studies of Nordic ecosystems: A review. *Nor. Geogr. Tidsskr. Nor. J. Geogr.* **2007**, *61*, 170–191. [CrossRef]
18. Lehmann, J.R.K.; Münchberger, W.; Knoth, C.; Blodau, C.; Nieberding, F.; Prinz, T.; Pancotto, V.A.; Kleinebecker, T. High-Resolution Classification of South Patagonian Peat Bog Microforms Reveals Potential Gaps in Up-Scaled CH4 Fluxes by use of Unmanned Aerial System (UAS) and CIR Imagery. *Remote Sens.* **2016**, *8*, 173. [CrossRef]
19. Kasprzak, M.; Migoń, P. DEM-based analysis of Geomorphology of a stepped sandstone plateau, Stołowe Mountains (SW Po-land). *Z. für Geomorphol.* **2015**, *58* (Suppl. S4), 247–270.
20. Wojewoda, J.; Białek, D.; Bucha, M.; Głuszyński, A.; Gotowała, R.; Krawczewski, J.; Schutty, B. Geology of the Góry Stołowe National Park–selected issues. In *Geoekologiczne Warunki Środowiska Przyrodniczego Parku Narodowego Gór Stołowych*; Chodak, T., Kabała, C., Kaszubkiewicz, J., Migoń, P., Wojewoda, J., Eds.; WIND: Wrocław, Poland; pp. 53–96. (In Polish)
21. Voigt, S.; Wagreich, M.; Surlyk, F.; Walaszczyk, I.; Uličný, D.; Čech, S.; Voigt, T.; Wiese, F.; Wilmsen, M.; Niebuhr, B.; et al. *The Geology of Central Europe – Mesozoic and Cenozoic*; McCann, T., Ed.; Geological Society of London: London, UK, 2008; Volume 6 (2), pp. 923–997.
22. Migoń, P.; Kasprzak, M. (Eds.) *Góry Stołowe. Geology, Landforms, Vegetation Patterns and Human Impact*; University of Wrocław: Wrocław, Poland, 2012. (In Polish)
23. Woronko, D. Conditions for the occurrence and functioning of wetlands in the Stołowe Mountains National Park). *Szczeliniec* **1998**, *2*, 23–29. (In Polish).
24. Dubicki, A.; Głowicki, B. Climate. In *Przyroda Parku Narodowego Gór Stołowych*; Witkowski, A., Pokryszko, B.M., Ciężkowski, W., Eds.; Wyd. Parku Narodowego Gór Stołowych: Kudowa-Zdrój, Poland, 2008; pp. 101–113. (In Polish)
25. Bogacz, A.; Roszkowicz, M. Influence of forest management on the changes of organic soil properties in marginal part of Kragle Mokradło Peatlands (Stołowe Mountains National Park). *Soil Sci. Annu.* **2010**, *61*, 15–20.
26. Glina, B.; Bogacz, A.; Pikus, H.; Pawluczuk, J. The impact of anthropopreassure and weather conditions on the mineral nitrogen content in the organic soils from fen peatlands (Stołowe Mountains, SW Poland). *Polish J. Soil Sci.* **2016**, *49*, 1. [CrossRef]
27. Glina, B.; Bogacz, A.; Woźniczka, P. Nitrogen mineralization in forestry drained peatland soils in the Stolowe Mountain National Park (Central Sudetes Mts). *Soil Sci. Annu.* **2016**, *67*, 64–72. [CrossRef]
28. Marek, S. Development of the Wielkie Torfowisko Batorowskie mountain mire as shown by palynological study. *Szczel-iniec* **1998**, *2*, 49–88. (In Polish).
29. Glina, B.; Malkiewicz, M.; Mendyk, Ł.; Bogacz, A.; Woźniczka, P. Human-affected disturbances in vegetation cover and peatland development in the late Holocene recorded in shallow mountain peatlands (Central Sudetes, SW Poland). *Boreas* **2016**, *46*, 294–307. [CrossRef]
30. Chodak, T. Spatial variability of soils and habitats in the Stolowe Mountains. In *Geoecological Conditions of the Stołowe Mountains National Park*; Chodak, T. Wind: Wroclaw, Poland, 2011; pp. 141–167.
31. Glina, B. Spatial variability of the shallow organic soils in the Stołowe Mountains as a result of anthropogenic transformations. Ph.D. Thesis, Wrocław University of Environmental and Life Sciences, Wrocław, Poland, 2014; pp. 1–208. (In Polish).

32. Glina, B.; Piernik, A.; Hulisz, P.; Mendyk, Ł.; Tomaszewska, K.; Podlaska, M.; Spychalski, W. Water or soil—What is the dominant driver controlling the vegetation pattern of degraded shallow mountain peatlands? *Land Degrad Dev.* **2019**, *30*, 1437–1448. [CrossRef]
33. Kurczyński, Z. Airborne Laser Scanning in Poland - Between Science and Practice. *Arch. Photogramm. Cartogr. Remote. Sens.* **2019**, *31*, 105–133. [CrossRef]
34. Conrad, O.; Bechtel, B.; Bock, M.; Dietrich, H.; Fischer, E.; Gerlitz, L.; Wehberg, J.; Wichmann, V.; Böhner, J. System for Automated Geoscientific Analyses (SAGA) v. 2.1. *Geosci. Model Dev.* **2015**, *8*, 1991–2007. [CrossRef]
35. Samouëlian, A.; Cousin, I.; Tabbagh, A.; Bruand, A.; Richard, G. Electrical resistivity survey in soil science: A review. *Soil Tillage Res.* **2005**, *83*, 173–193. [CrossRef]
36. Schrott, L.; Sass, S. Application of field geophysics in geomorphology: Advances and limitations exemplified by case studies. *Geomorphology* **2008**, *93*, 55–73. [CrossRef]
37. Van Dam, R.L. Landform characterization using geophysics—Recent advances, applications, and emerging tools. *Geomorphology* **2012**, *137*, 57–73. [CrossRef]
38. Loke, M.H.; Chambers, J.E.; Rucker, D.F.; Kuras, O.; Wilkinson, P.B. Recent developments in the direct-current geoelectrical imaging method. *J. Appl. Geophys.* **2013**, *95*, 135–156. [CrossRef]
39. Kasprzak, M. Application of high-resolution electrical resistivity tomography to patterned ground (Wedel Jarlsberg Land, SW Spitsbergen). *Polar Res.* **2015**, *34*, 25678. [CrossRef]
40. Loke, M.H. *Electrical Imaging Surveys for Environmental and Engineering Studies*; A practical guide to 2-D and 3-D surveys; Geotomo: Penang, Malaysia, 2000.
41. Reynolds, J.M. Electrical Resistivity Methods. In *An Introduction to Applied and Environmental Geophysics*, 2nd ed.; Wiley: Chichester, UK, 2011; pp. 289–372.
42. Daniels, D. *Ground Penetrating Radar*, 2nd ed.; The Institution of Electrical Engineers: London, UK, 2004; pp. 1–734.
43. Utsi, E.C. Ground Penetrating Radar. In *Theory and Practice*; Elsevier: Kidlington, UK, 2017; pp. 1–205.
44. Warner, B.G.; Nobes, D.C.; Theimer, B.D. An application of ground-penetrating radar to peat stratigraphy of Ellice Swamp, Southwest Ontario. *Can. J. Earth Sci.* **1990**, *27*, 932–938. [CrossRef]
45. Theimer, B.D.; Nobes, D.C.; Warner, B.G. A study of the geoelectrical properties of peatlands and their influence on ground-penetrating radar surveying. *Geophys. Prospect.* **1994**, *42*, 179–209. [CrossRef]
46. Comas, X.; Slater, L.; Reeve, A. Stratigraphic controls on pool formation in a domed bog inferred from ground penetrating radar (GPR). *J. Hydrol.* **2005**, *315*, 40–51. [CrossRef]